

# AAV2-antiVEGFscFv gene therapy for retinal neovascularization

Ni Han,<sup>1,4</sup> Xin Xu,<sup>1,4</sup> Ying Liu,<sup>2</sup> and Guangzuo Luo<sup>1,3</sup>

<sup>1</sup>Institute of Health Sciences, China Medical University, Shenyang 110122, China; <sup>2</sup>Department of Biochemistry and Molecular Biology, China Medical University, Shenyang 110122, China; <sup>3</sup>Bionce Biotechnology, Ltd., Nanjing 210061, China

**Retinal neovascularization (NV) may lead to irreversible vision impairment, the main treatment for which is the inhibition of vascular endothelial growth factor (VEGF). Existing drugs show limited clinical benefits because of their high prices and short half-lives, which increase the financial burden and medical risks to patients. Gene therapy on the basis of adeno-associated viruses is a promising approach to overcome these limitations because of the nonintegrative nature, low immunogenicity, and potential long-term gene expression of adeno-associated viruses. In this study, we constructed a novel recombinant adeno-associated virus with the single-chain fragment variable (scFv) fragment of the anti-VEGF antibody, AAV2-antiVEGFscFv, consisting of the VH and VL structural domains of IgG. AAV2-antiVEGFscFv effectively inhibited NV, retinal leakage, and retinal detachment in oxygen-induced retinopathy (OIR) mice, *Tet/opsin/VEGF* double-transgenic mice, and VEGF-induced rabbit NV models. AAV2-antiVEGFscFv also significantly suppressed VEGF-induced inflammation. Furthermore, we showed that AAV2-antiVEGFscFv could be sustainably expressed for a prolonged period and exhibited low immunotoxicity *in vivo*. This study indicates that AAV2-antiVEGFscFv could be a potential approach for NV treatment and provides strong support for preclinical research.**

## INTRODUCTION

Retinal neovascularization (NV) is associated with a variety of retinal diseases, such as neovascular age-related macular degeneration (nAMD), retinopathy of prematurity (ROP), and pathological myopia.<sup>1</sup> NV can cause severe tissue edema, hemorrhage, fibrotic scar formation, retinal detachment, and other pathological changes, resulting in loss of central vision, visual distortion, and reduced contrast sensitivity, eventually progressing to irreversible vision loss and blindness.<sup>2,3</sup>

NV shares similar characteristics with pathological angiogenesis elsewhere in the body, exhibiting features including hypoxia, endothelial proliferation and migration, elevated vascular permeability, and inflammation, all processes in which vascular endothelial growth factor (VEGF) plays a crucial role.<sup>4</sup> Hence, VEGF is a key target for therapeutic intervention in the treatment of patients with NV-associated diseases. Currently available anti-VEGF drugs include ranibizumab, brodalumab, aflibercept, and conbercept, which are widely used in the treatment of patients with NV and retinal leakage.<sup>5</sup> However, their high pri-

ces and short half-lives limit the clinical benefits of existing anti-VEGF drugs. Patients need intraocular injections of anti-VEGF drugs every 1 to 3 months to maximize and maintain efficacy, a process that imposes heavy financial burden and high medical risks on patients.<sup>6</sup> Therefore, it is necessary to develop an anti-VEGF drug with a sustainable expression pattern and reduce the frequency of administration.

Adeno-associated virus (AAV) vectors are an appealing platform because of their nonintegrative nature, low immunogenicity, and long-term gene expression.<sup>7,8</sup> Early results from the most recent anti-VEGF gene therapy clinical studies, one using surgical subretinal delivery carried out in the operating room (RGX-314), one using in-office IVI (ADVM-022),<sup>9,10</sup> and the other IVI AAV-based gene therapy designed to express aflibercept (4D-150) (NCT05197270), have shown efficacy and a good safety profile in clinical trials for nAMD and demonstrated the potential of one-time gene therapy to provide long-lasting control of NV-associated diseases.<sup>7,11</sup>

In this study, we developed a novel recombinant AAV-based therapy for NV, AAV2-antiVEGFscFv, which was optimized for efficient and long-term protein expression. After assessing its activity *in vitro*, we evaluated the therapeutic efficiency of AAV2-antiVEGFscFv in oxygen-induced retinopathy (OIR) mice, *Tet/opsin/VEGF* double-transgenic mice, and a VEGF-induced rabbit NV model. We also evaluated the sustainability of expression and immunotoxicity of AAV2-antiVEGFscFv in C57BL/6J mice. The results of this study support further preclinical research of AAV2-antiVEGFscFv vector as potentially safe and effective long-term treatment option for NV-associated diseases.

## RESULTS

### Construction and *in vitro* testing of AAV2-antiVEGFscFv

AAV2-antiVEGFscFv uses the AAV serotype 2 (AAV2) capsid as a vector for delivering and encoding the antiVEGFscFv antibody, a VEGF

Received 19 April 2023; accepted 25 October 2023;  
<https://doi.org/10.1016/j.omtm.2023.101145>.

<sup>4</sup>These authors contributed equally

**Correspondence:** Ying Liu, Department of Biochemistry and Molecular Biology, China Medical University, Shenyang 110122, China.

**E-mail:** [liuying@cmu.edu.cn](mailto:liuying@cmu.edu.cn)

**Correspondence:** Guangzuo Luo, Institute of Health Sciences, China Medical University, Shenyang 110122, China.

**E-mail:** [gzluo@cmu.edu.cn](mailto:gzluo@cmu.edu.cn)



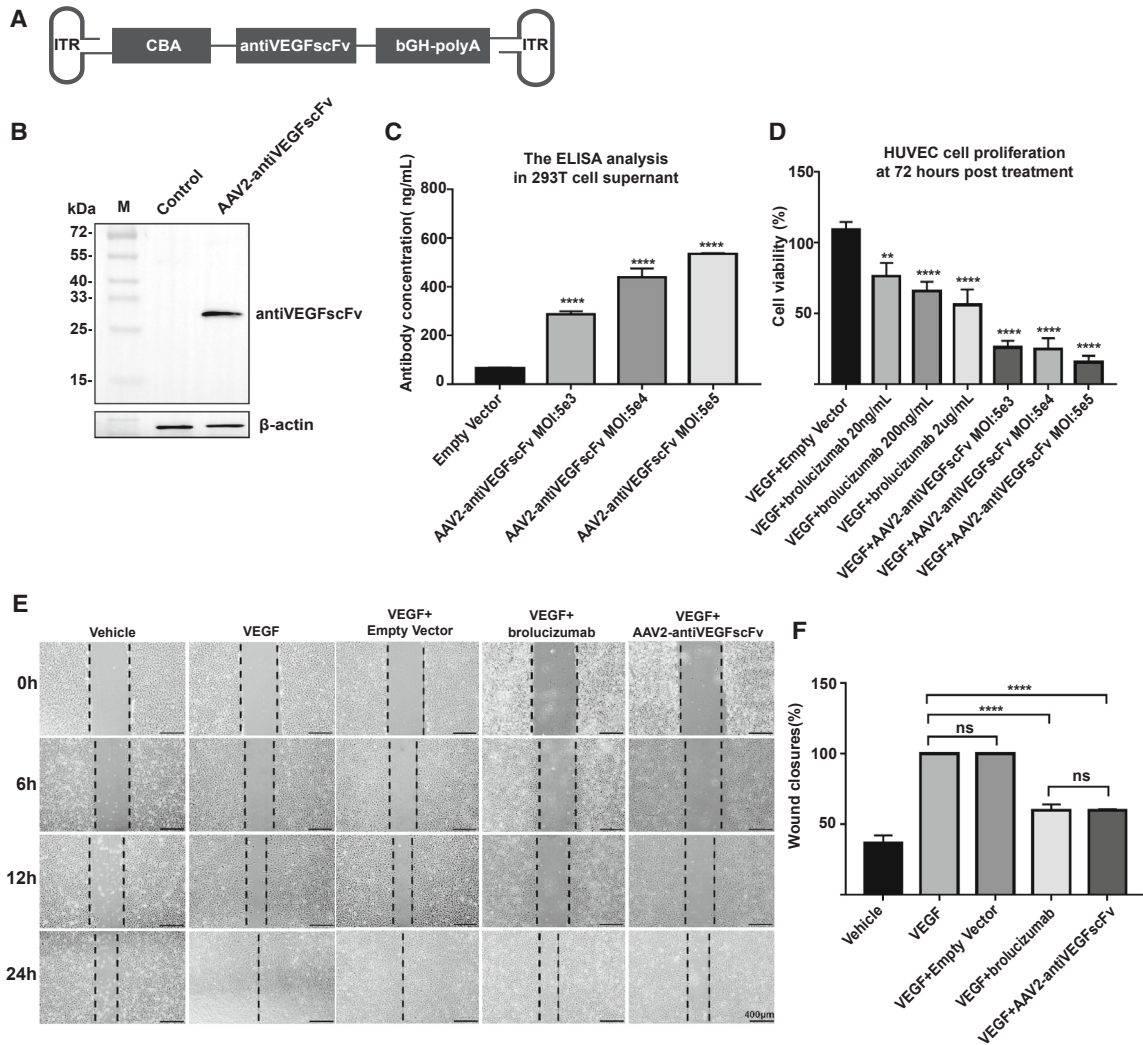


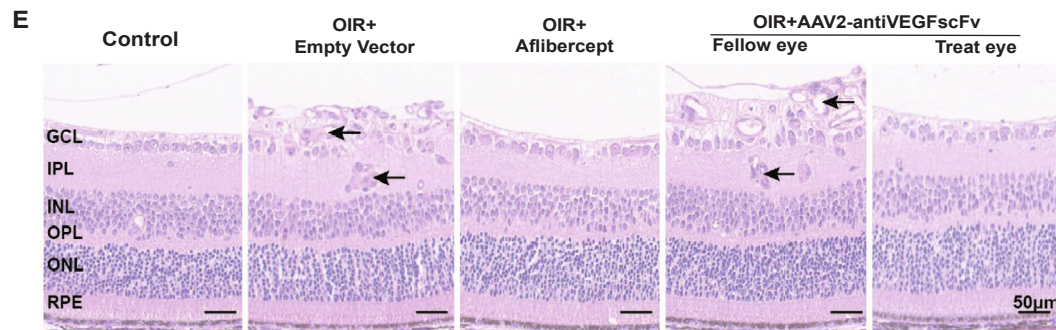
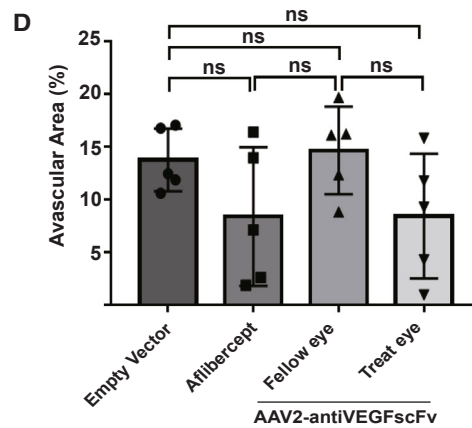
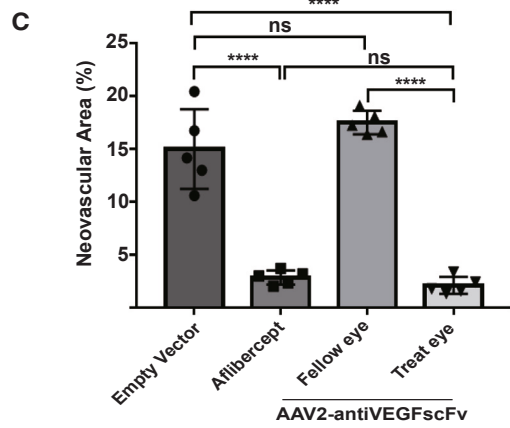
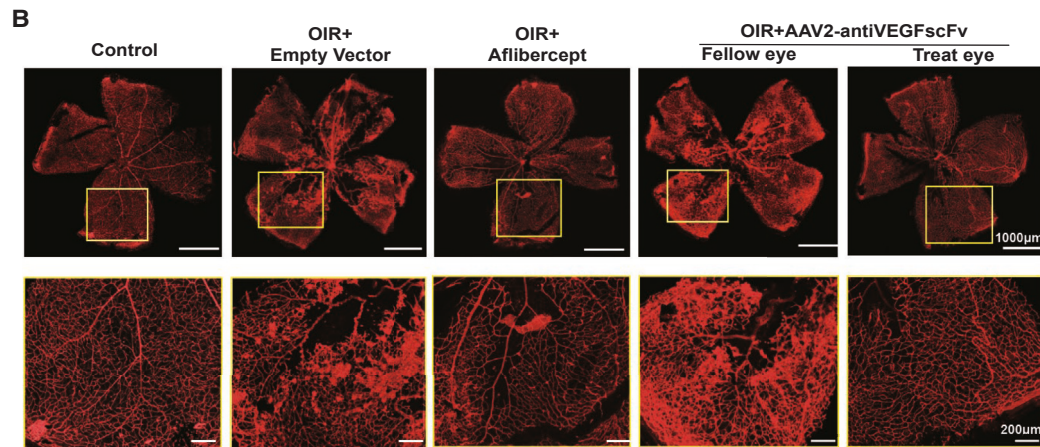
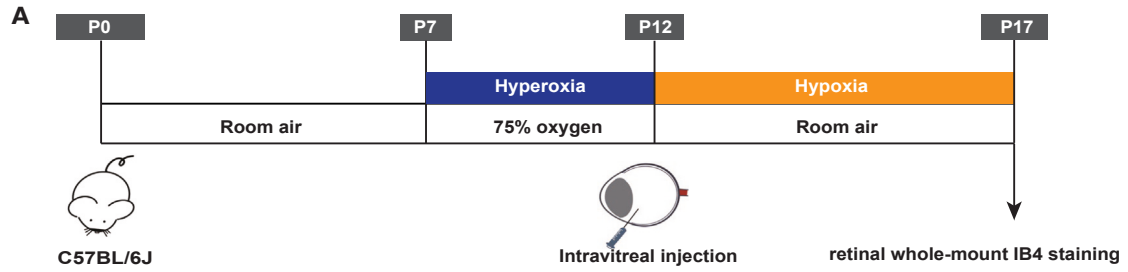
**Figure 1. Construction and *in vitro* testing of AAV2-antiVEGFscFv**

(A) Schematic representation of AAV2-antiVEGFscFv vector. ITR, inverted terminal repeat of AAV2. CBA, CBA promoter. antiVEGFscFv, single-chain antibody. bGH-pA, bovine growth hormone polyadenylation signal. (B) Demonstrating the expression of antiVEGFscFv antibodies secreted by AAV2-antiVEGFscFv-transduced cells by western blot. HEK293T cells were transduced by AAV2-antiVEGFscFv or a control empty vector. (C) Antigen specificity of antiVEGFscFv antibodies secreted by AAV2-antiVEGFscFv-transduced cells. 293T cells were transduced by AAV2-antiVEGFscFv at different MOIs or a control empty vector, and the supernatants were assayed for activity using ELISA. The plates were coated with hVEGF. (D) Measurement of 490 nm values of HUVECs in 96-well plates 1 h after added CCK8 reagent at 48 h after treatment with vehicle (blank), exogenous VEGF (50 ng/mL) on its own or combined with empty vector (MOI = 1:100,000), brotlicuzumab (2 μg/mL, 200 ng/mL, or 20 ng/mL), or AAV2-antiVEGFscFv (MOI = 1:500,000, MOI = 1:50,000, and MOI = 1:5,000). (E) Representative images of HUVEC wound healing assays were acquired at 0, 6, 12, and 24 h after treatment with vehicle (blank), exogenous VEGF (50 ng/mL) on its own or combined with empty vector (MOI = 1:100,000), brotlicuzumab (100 ng/mL), or AAV2-antiVEGFscFv (MOI = 1:100,000). (F) Quantitative analysis of HUVEC wound healing assays at 24 h after treatment. One-way ANOVA was used for statistical analysis and data are mean ± standard error. \*p < 0.05, \*\*p < 0.01, \*\*\*p < 0.001, and \*\*\*\*p < 0.0001; ns, not significant.

antibody, in single-chain fragment variable (scFv) format. Brotilcuzumab was the source of the scFv sequence. A schematic representation of the sequence of AAV2-antiVEGFscFv is shown in Figure 1A. The cDNA encoding antiVEGFscFv was inserted into an expression cassette containing the cytometric bead array (CBA) promoter to drive its expression.

We validated the correct assembly using western blot and an ELISA to detect the expression and antigen specificity of the antiVEGFscFv an-

tibodies secreted by AAV2-antiVEGFscFv-transduced human embryonic kidney 293T (HEK293T) cells. As shown in the results, the specific bands could be detected in transduced cells and cell supernatants by western blot, and the VEGF-binding activity could be proved in cell supernatants using ELISA (Figures 1B and 1C). To evaluate the anti-VEGF effect of AAV2-antiVEGFscFv *in vitro*, cell proliferation and migration assays were performed using VEGF-dependent human umbilical vein endothelial cells (HUVECs). As shown in



(legend on next page)

Figures 1D–1F, the brolicuzumab (positive control) and AAV2-antiVEGFscFv groups had dose-dependent inhibitory effects on HUVEC proliferation and migration. Compared with positive control, AAV2-antiVEGFscFv had better effect on cell proliferation and a similar effect on cell migration.

#### Single intravitreal injection of AAV2-antiVEGFscFv suppresses NV in OIR mice

Considering that hypoxia is one of the features of NV, the OIR mouse model was used to evaluate the anti-angiogenesis effect of AAV2-antiVEGFscFv *in vivo*.<sup>4</sup> Pups of C57BL/6J mice at postnatal day 7 (P7) along with their nursing mothers were placed in 75% oxygen for 5 days (P12) and then returned to room atmosphere for another 5 days (P17). The mice received intravitreal injections of 1  $\mu$ L PBS (control group),  $2.5 \times 10^8$  GC empty vector, 40  $\mu$ g aflibercept (positive control group), or  $2.5 \times 10^8$  GC AAV2-antiVEGFscFv at P7. Retinal vessels were investigated using whole-mount IB4 lectin staining performed at P17 (Figure 2B, lower image). Unlike normal retinal vasculature in the control group, neovascular and avascular areas were observed in the retinas of OIR mice. After AAV2-antiVEGFscFv treatment, neovascular areas were markedly reduced, comparable with those in the positive control group (Figure 2C). However, there was no significant reduction in the avascular areas in the AAV2-antiVEGFscFv group, similar to the positive control group (Figure 2D). To further analyze the effect of AAV2-antiVEGFscFv on pathologies, we performed H&E staining of mouse eyes. Unlike the normal superficial retinal vascular network (SCP) in the nerve fiber and inner plexiform layers of the control group, there were abnormal blood vessels growing into the vitreous cavity and enlarged blood vessels (Figure 2E, black arrows) within the retina of the empty vector group and the fellow eye in the AAV2-antiVEGFscFv group, indicating retinal NV (RNV). After the administration of aflibercept or AAV2-antiVEGFscFv, neatly arranged cells in the nerve fiber layer and decreased abnormal SCP were observed, suggesting an inhibitory effect of AAV2-antiVEGFscFv on RNV, comparable with that of aflibercept.

#### Single intravitreal injection of AAV2-antiVEGFscFv improves vascular pathologies in *Tet/opsin/VEGF* mice

*Tet/opsin/VEGF* double-transgenic mice, in which the tet-on system and the rhodopsin promoter provide doxycycline-inducible expression of VEGF<sub>165</sub>, develop exudative retinal detachment within 4 days of starting 2 mg/mL doxycycline in drinking water.<sup>12</sup> Two weeks after intravitreal injection of 2  $\mu$ L PBS,  $5 \times 10^8$  GC empty vector, or intravitreal monocular injection of  $5 \times 10^8$  GC AAV2-antiVEGFscFv into *Tet/opsin/VEGF* double-transgenic mice, 2 mg/mL doxycycline was added to their drinking water. Ten days af-

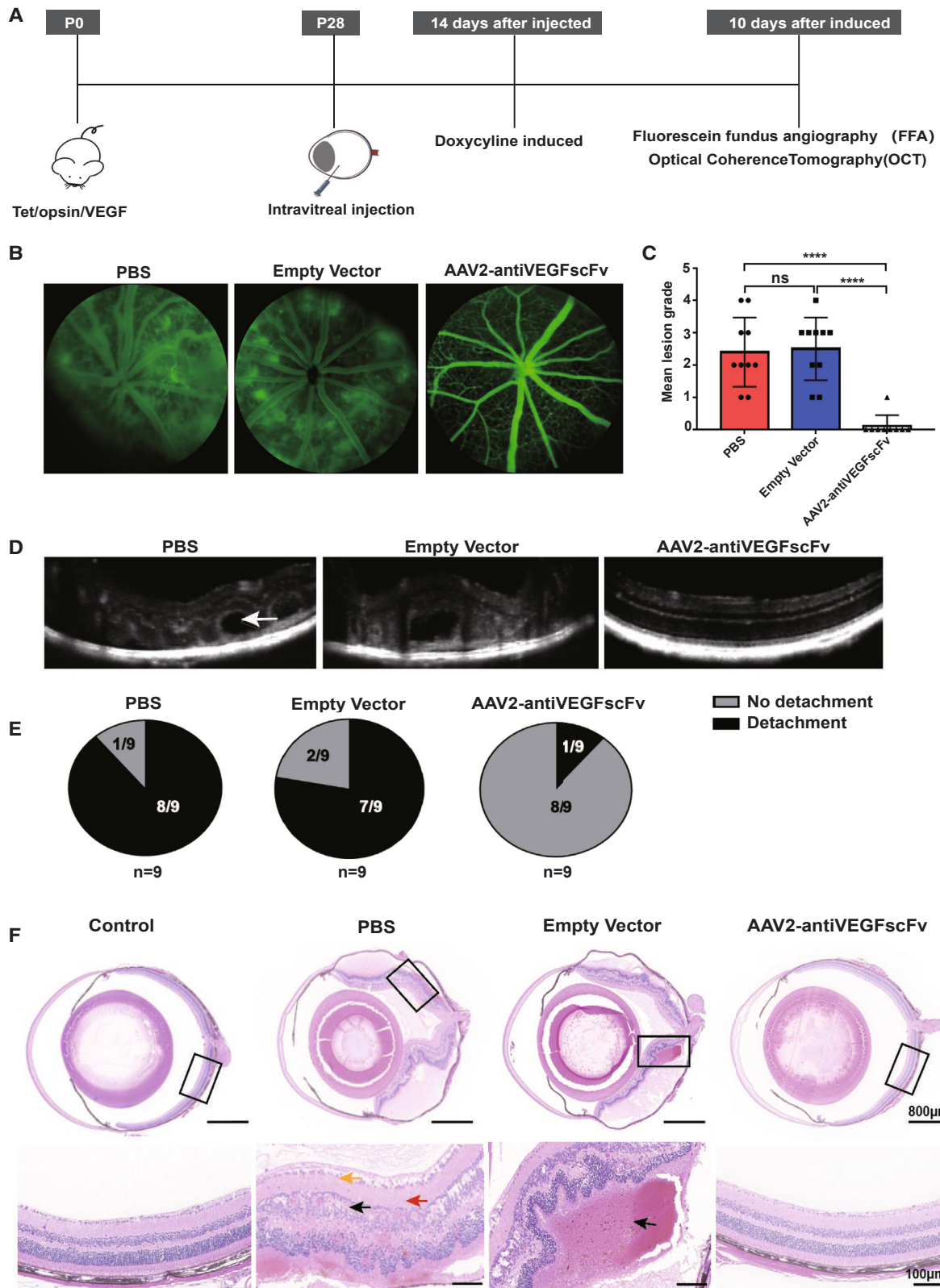
ter doxycycline induction, fundus fluorescein angiography (FFA) and optical coherence tomography (OCT) were performed to evaluate the effect of AAV2-antiVEGFscFv on fundus vascular leakage (Figure 3A). Fluorescein leakage was evident in the eyes of *Tet/opsin/VEGF* mice after induction, indicating increased vascular permeability induced by doxycycline. FFA demonstrated that the size and number areas with fluorescein outside of the blood vessels significantly decreased in the AAV2-antiVEGFscFv group, suggesting that AAV2-antiVEGFscFv suppressed fluorescein leakage by decreasing vascular permeability (Figures 3B and 3C). Four days after induction, eight of nine eyes administered an intravitreal injection of PBS and seven of nine eyes injected with empty vector had total retinal detachment. OCT suggested that unlike in the mice of PBS or empty vector group, the retinal detachment was improved in the mice of AAV2-antiVEGFscFv group, with only one of nine eyes exhibiting it (Figures 3D and 3E). To further understand the pathophysiological changes in AAV2-antiVEGFscFv treated *Tet/opsin/VEGF* mice, we analyzed the histological cross-sections of these eyes. Compared with the control group, H&E staining showed a disordered arrangement of retinal cells and presented massive pathologies, including edema (Figure 3F), significant subretinal and intraretinal hemorrhages, and retinal detachment, in the retina of the PBS group or the empty vector group mice. Following treatment with AAV2-antiVEGFscFv, the pathologies described above improved remarkably (Figure 3F).

#### AAV2-antiVEGFscFv reduces VEGF-induced inflammation in *Tet/opsin/VEGF* mice

Recent studies have demonstrated that inflammation is an important mechanism that promotes the formation of choroidal NV (CNV), which is regulated by inflammatory cytokines.<sup>13,14</sup> Considering the efficacy of AAV2-antiVEGFscFv on NV, we speculated that it could inhibit inflammation and evaluated it in *Tet/opsin/VEGF* mice. We first verified the anti-VEGF effect of AAV2-antiVEGFscFv *in vivo* using western blot. Compared with the PBS group or the empty vector group, the relative expression of VEGFR2 and phosphorylated VEGFR2 (pVEGFR2) was significantly decreased in the eyes of the AAV2-antiVEGFscFv group, indicating an inhibitory effect of AAV2-antiVEGFscFv on VEGFR2 protein phosphorylation (Figure 4A). Then, we performed immunofluorescence, immunohistochemistry (IHC), and ELISA to evaluate the effect of AAV2-antiVEGFscFv on CNV-associated inflammation in *Tet/opsin/VEGF* mice. Macrophages have been considered the main type of infiltrating inflammatory cells in nAMD eyes.<sup>15,16</sup> Therefore, we evaluated the macrophage infiltration by immunofluorescence. As shown in Figure 4B, there was obvious recruitment and infiltration of macrophage in the retina of the PBS and empty vector groups, which was absent in the

#### Figure 2. AAV2-antiVEGFscFv inhibits retinal vascular neogenesis in OIR mice

(A) Schematic representation of the schedule of OIR induction, administration, and subsequent analysis. (B) Representative retinal whole-mount IB4 staining of each group on P17. Below is an enlarged view of the neovascularize area.  $n = 5$ . (C) The neovascularize areas were quantified as the ratio of the central avascular area to the whole retinal area.  $n = 5$ . (D) The avascular areas were quantified as the ratio of the central avascular area to the whole retinal area.  $n = 5$ . (E) Representative image of H&E staining of a mouse eye, with black arrows indicating neovascularization.  $n = 5$ . One-way ANOVA was used for statistical analysis, and data are mean  $\pm$  standard error. \*\*\* $p < 0.001$ ; ns, not significant. OIR, oxygen-induced retinopathy.



(legend on next page)

AAV2-antiVEGFscFv group, consistent with the positive control group. Furthermore, compared with the upregulated expression of the inflammatory factors TNF- $\alpha$ , IL-1, and IL-6 in the retina of the PBS group and the empty vector group, there was a significant downregulation in the AAV2-antiVEGFscFv group (Figures 5A and 5D). These results revealed that AAV2-antiVEGFscFv suppressed VEGF-induced inflammation by reducing the recruitment and infiltration of macrophages and downregulating the expression of inflammatory factors.

### Single subretinal injection of AAV2-antiVEGFscFv blocks vascular leakage in VEGF-induced rabbit NV model

The encouraging results regarding the anti-angiogenic efficacy of AAV2-antiVEGFscFv led us to extend the study to a rabbit NV model of VEGF-induced retinal vascular leakage. Male Dutch black-banded rabbits aged 3–6 months were selected for subretinal monocular injection of  $1.5 \times 10^{10}$  GC empty vector or AAV2-antiVEGFscFv (day 0 [D0]). As shown in Figure 6A, we performed intravitreal monocular injection of 50  $\mu$ L (40 mg/mL) aflibercept in the eye at D12, which was used as the positive control. The fellow eye was untreated and served as the control. Then, intravitreal injection of 50  $\mu$ L (1.8  $\mu$ g/eye) human-derived VEGFA<sub>165</sub> was performed at D14 to construct the rabbit NV model.<sup>17</sup> To evaluate the efficacy of AAV2-antiVEGFscFv in the rabbit NV model, the retinal vascular leakage at D17 and D21 was evaluated using FFA. After induction with human-derived VEGFA<sub>165</sub>, there was significant vascular leakage in the eyes of the empty vector group, regardless of whether the empty vector was administered. Compared with the fellow eye, the vascular leakage in the eyes treated with aflibercept or AAV2-antiVEGFscFv was remarkably reduced (Figures 6B–6E). In addition, the inhibitory effects of aflibercept or AAV2-antiVEGFscFv increased with treatment time.

### Long-term expression and safety of AAV2-antiVEGFscFv

Long-term expression is one of the outstanding advantages of gene therapy. Therefore, on the basis of *Tet/opsin/VEGF* mouse model, we detected the antiVEGFscFv expression in the retinas at different time points after AAV2-antiVEGFscFv injection. As shown in Figure 7A, antiVEGFscFv began to express at 1 week after AAV2-antiVEGFscFv-injection, with a peak 4 weeks after injection. In addition, FFA showed a significant inhibitory effect of AAV2-antiVEGFscFv on vascular leakage in *Tet/opsin/VEGF* mouse model at 12 weeks after injection, indicating the long-term expression of AAV2-antiVEGFscFv. Furthermore, to assess the safety of AAV2-antiVEGFscFv *in vivo*, we evaluated its influence on retinal structure and function using OCT and electroretinography (ERG). C57BL/6J mice at the age of 4 weeks were selected for subretinal injection of  $1 \times 10^9$  GC of empty vector, AAV2-antiVEGFscFv, or 2  $\mu$ L PBS, which was used as a control. AAV2-

antiVEGFscFv caused a bleb in the retina at the beginning of injection. However, with the absorption of the drug, the bleb in the retina returned to normal and did not differ from those in the PBS group at 4 weeks after injection (Figure 7B). In addition, there was no significant reduction in A- and B-wave amplitudes and implicit times in the AAV2-antiVEGFscFv group at 4 weeks after injection, indicating that AAV2-antiVEGFscFv treatment did not affect retinal function in C57BL/6J mice (Figure 7C). AAV-induced immune response may lead to significant inflammation and/or deterioration of vision.<sup>18</sup> Therefore, we detected the expression of inflammatory factors in the retinas of C57BL/6J mice to evaluate the safety of AAV2-antiVEGFscFv. Compared with the PBS or empty vector groups, there was no significant difference in the AAV2-antiVEGFscFv group, indicating that AAV2-antiVEGFscFv may not cause inflammation in the retinas (Figure 7D).

## DISCUSSION

Current anti-angiogenic drugs commonly used to treat NV-related retinal diseases include bevacizumab and ranibizumab, which are very effective at suppressing NV and retinal vascular leakage and alleviating visual impairment.<sup>19–22</sup> However, the short half-lives of antibody drugs cause patients to frequently undergo ocular injection for long-term treatment, seriously affecting their quality of life.<sup>6,23</sup> Therefore, it is necessary to find an effective means to reduce the frequency of administration while ensuring long-term therapeutic effect and safety. Gene therapy based on AAV vectors has the potential to overcome these limitations because of the long-term gene expression following a single administration.<sup>7</sup>

In this study, we constructed a novel recombinant AAV-based therapy for NV, AAV2-antiVEGFscFv, consisting of only the VH and VL structural domains of IgG, which encodes brolocizumab. Brolocizumab is a novel scFv antibody that inhibits all isoforms of VEGFA and prevents binding of this ligand to VEGFR1 and VEGFR2.<sup>24</sup> Compared with the full antibody (bevacizumab) or the Fab fragment (ranibizumab), brolocizumab is a small molecular humanized antibody with only 26 kDa, half the size of ranibizumab, which is suggested to have more tissue penetration in retina.<sup>25,26</sup> It has been shown that Fc $\gamma$  receptor upregulation in age-related macular degeneration (AMD) produces immune complex-mediated inflammation.<sup>27,28</sup> Therefore, in theory, antibodies of scFv structure without the Fc structure could reduce such immune responses.

Local and systemic immune responses and ocular inflammation have been reported after clinical ocular delivery of AAV.<sup>18</sup> A detailed understanding of local AAV-induced immune responses in the eye, which are called gene therapy-associated uveitis (GTU), is particularly

### Figure 3. AAV2-antiVEGFscFv efficacy experiments in *Tet/opsin/VEGF* transgenic mice

(A) Flowchart of the experiment. (B) Representative pictures of FFA. The area with strong fluorescence signal is retinal vascular leakage, and the effect of drug on leakage was assessed using fundus fluorescein angiography (FFA). The fluorescence signal of eyes injected with AAV (n = 9) was significantly lower than that of the control groups injected with PBS (n = 10) or empty vector (n = 10). (C) A quantitative statistical plot of (B), by scoring the fluorescence leakage in each eye n = 9. One eye of the mouse in the AAV2-antiVEGFscFv group was not photographed because of cataracts or vitreous opacity. (D) A representative picture of OCT, where the area of retinal detachment (white arrow) can be observed in the PBS and Empty vector groups, but not in the AAV-injected group. n = 9. (E) Statistical plot of (D), counting the retinal detachment rate of each group. n = 9. (F) Representative pictures of eye sections taken for H&E staining after execution of mice. n = 3.

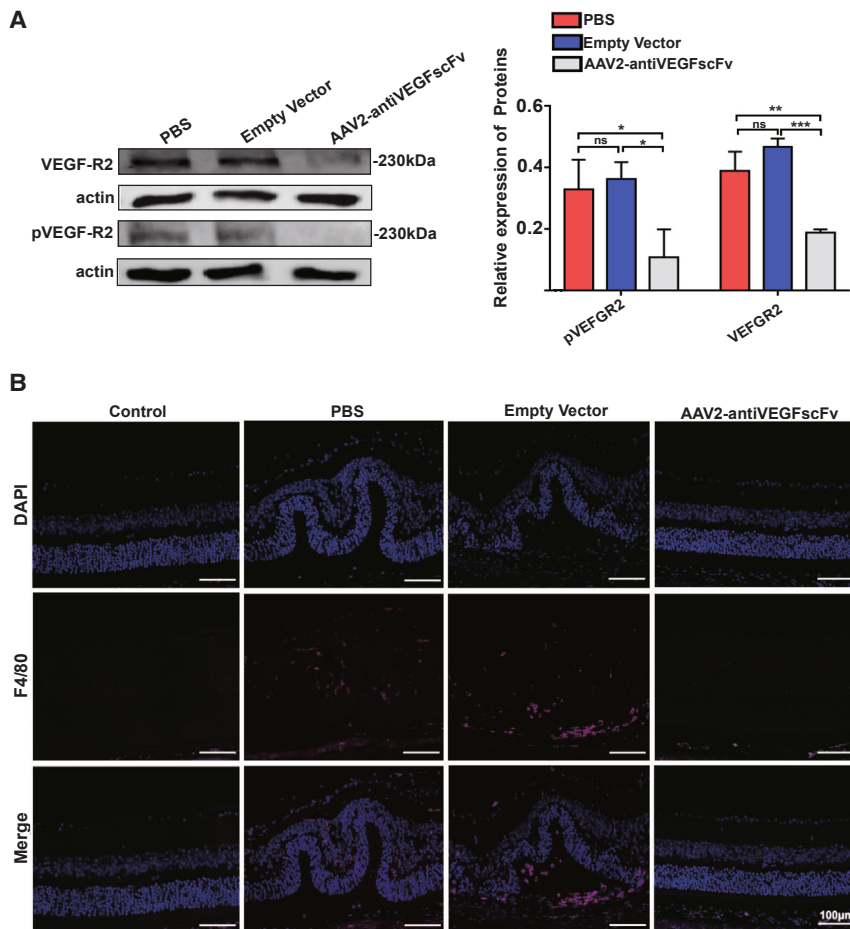


**Figure 4. AAV2-antiVEGFscFv downregulates F4/80 signaling, VEGFR2, and activation of VEGFR2 in doxycycline-induced *Tet/opsin/VEGF* mice**

(A) Western blot quantitative analysis of the relative expression of VEGFR2 and phosphorylated VEGFR2 (pVEGFR2) in the retinas of mice 10 days after doxycycline induction in each treatment group, one retina as a separate sample. One-way ANOVA was used for statistical analysis, and data are mean  $\pm$  standard error. \* $p < 0.05$ , \*\* $p < 0.01$ , and \*\*\* $p < 0.001$ ; ns, not significant.  $n = 3$ . (B) Immunofluorescence analysis of F4/80 expression in the eye of mice 10 days after doxycycline induction in each treatment group, with wild-type C57BL/6 mice serving as a control.

antiVEGFscFv in OIR mouse model and *Tet/opsin/VEGF* mouse model. We did not evaluate the efficacy of subretinal injection in the mouse disease model, mainly because the eyes in the disease model are very fragile, and subretinal injection may cause retinal detachment. Indeed, recently subretinal injection was found to result in the adverse events potentially associated with subclinical immune response. The development of retinal atrophy has been reported in many patients after subretinal gene therapy with subretinal injection, leading to photoreceptor loss both within and outside of the bleb area.<sup>36</sup> In addition, a number of patients were reported to develop intraocular inflammation, which was treatable with immunosuppressant therapy, following the administration of subretinal injection.<sup>37</sup> We

important because they can lead to clinically significant inflammation and deterioration of vision.<sup>18,29,30</sup> Depending on factors such as carrier type, route of administration, and dose, GTU can include retinal toxicity, innate immune response, and adaptive immune response. The carrier type used in this study was AAV2, which is the first AAV vector discovered in adenoviruses in the 1960s. Besides, of the many serotypes, AAV2 has been the most thoroughly studied.<sup>31</sup> In addition, Luxturna, the only ophthalmic gene therapy drug on the market, uses the AAV2 serotype, and no major adverse events have been observed in clinical use to date.<sup>32,33</sup> The evaluation of retinal TNF- $\alpha$ , IL-1, or IL-6 expression indicated that AAV2-antiVEGFscFv may not lead to antigen specific adaptive immune response, which is mainly caused by AAV-mediated PRR signaling.<sup>18,34</sup>

However, the safety assessment of AAV2-antiVEGFscFv is far from sufficient. The administration of gene therapy is also one of important factors affecting the inflammatory response. In retinal gene therapy, the AAV vector is typically applied either by intravitreal injection or by subretinal injection.<sup>18</sup> Compared with intravitreal injection, subretinal injection with the same dose and carrier serotype has a higher transduction efficiency for intraretinal cells.<sup>35</sup> In this study, we evaluated the efficiency of intravitreally injected AAV2-

used subretinal injection in a larger animal model (rabbit CNV model) and evaluated its safety in wild-type mice, despite numerous defects. Compared with subretinal injection, vitreous injection can cause an increase in aqueous humor and systemic serum load, which increases the possibility of inflammation.<sup>38</sup> In addition, vitreous injections exhibit a stronger AAV2-neutralizing antibody response than subretinal injections, potentially reducing drug efficacy.<sup>39</sup> The administration of AAV2-antiVEGFscFv in the future clinical use needs more exploration on the basis of large animal models, such as the cynomolgus monkey CNV model.

Previous studies have demonstrated the therapeutic efficacy of scFv and immunoglobulin G1 (IgG1) format antibodies in CNV mouse models. Although laser-induced CNV mouse models are similar to human retinal diseases, they are transient and self-healing.<sup>40</sup> For the long-term evaluation of AAV2-antiVEGFscFv, we first used OIR mice, a vascular wound healing model induced by hypoxia.<sup>41,42</sup> We found that the vitreous cavity injection of  $2.5 \times 10^8$  GC AAV2-antiVEGFscFv strongly inhibited NV in OIR mice. Of note, AAV2-antiVEGFscFv had no significant effect on the size of avascular areas (Figure 2D), suggesting that this anti-angiogenic effect targeted only abnormal NV, rather than the repair of normal retinal vasculature.<sup>41</sup>

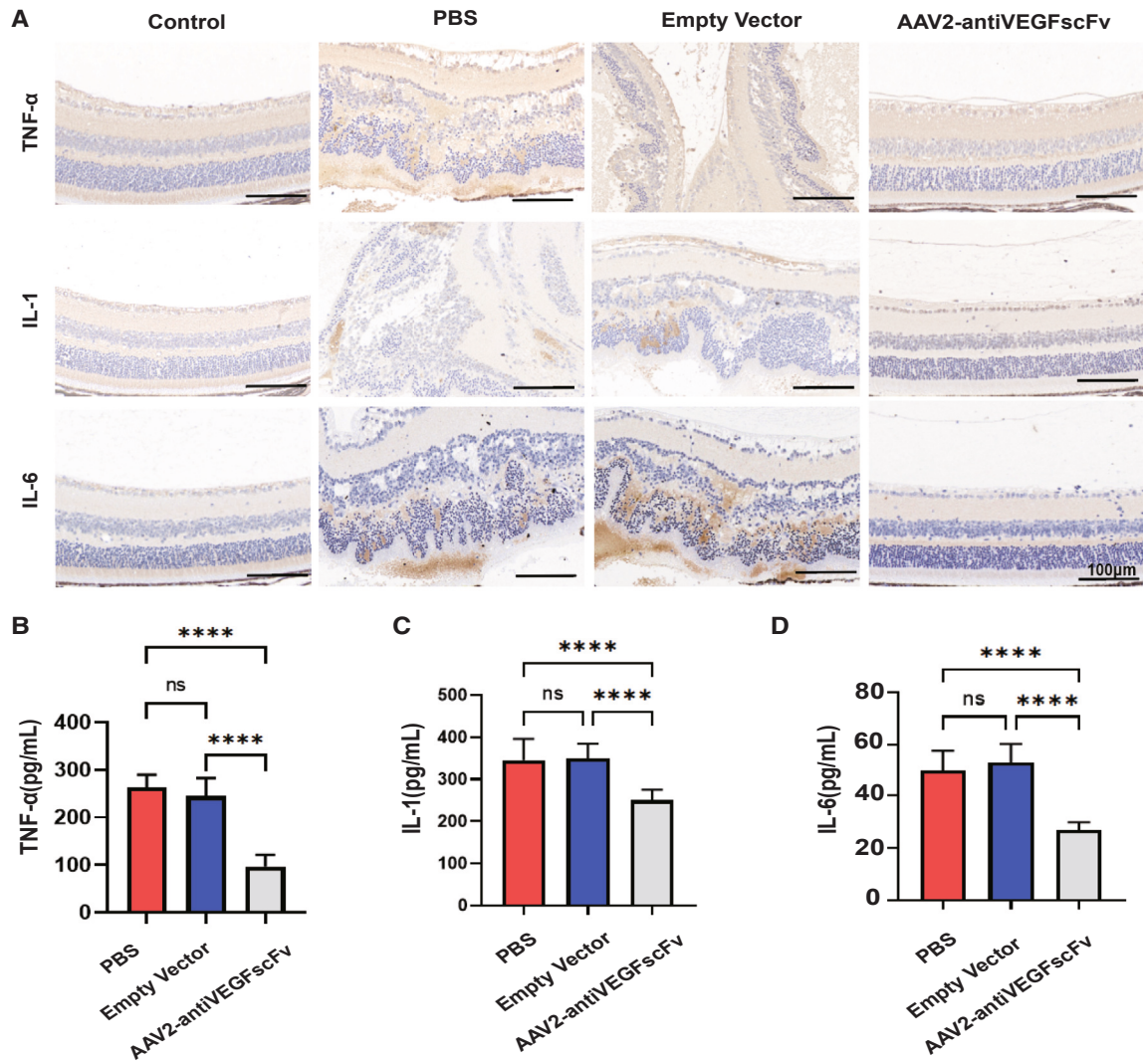


**Figure 5. AAV2-antiVEGFscFv downregulates expression of inflammatory factors in the eyes of doxycycline-induced *Tet/opsin/VEGF* mice**

(A) Immunohistochemical analysis of the expression of inflammatory factors in the eyes of mice 10 days after doxycycline induction in each treatment group.  $n = 3$ . (B–D) The expression of inflammatory factors in the retinas of mice.  $n = 3$ . One-way ANOVA was used for statistical analysis, and data are mean  $\pm$  standard error. \*\* $p < 0.01$  and \*\*\* $p < 0.001$ ; ns, not significant.

Compared with OIR mice, *Tet/opsin/VEGF* mice, induced by overexpression of human VEGF<sub>165</sub>, could better simulate the progression of clinical chronic disease from angiogenesis and leakage to retinal detachment.<sup>43</sup> In *Tet/opsin/VEGF* mice, vitreous cavity injection of  $5 \times 10^8$  GC AAV2-antiVEGFscFv significantly reduced vascular leakage and even retinal detachment, indicating that AAV2-antiVEGFscFv has a protective effect on severe ocular vascular lesions. These encouraging results regarding the anti-angiogenic efficacy of AAV2-antiVEGFscFv led us to extend the study to large animal models. Compared with the non-human primate CNV model, the rabbit NV model avoids the expense and ethical issues of the primate model, although the rabbit retina is supplied by a medullary ray, unlike the vascular supply of the retina to primates and rodents.<sup>44</sup> In the human-derived VEGF-induced rabbit NV model,

leakage was suppressed by subretinal injection of  $1.5 \times 10^{10}$  GC AAV2-antiVEGFscFv group, although it was not statistically different at D17 compared with the empty vector group. However, at D21, leakage was suppressed compared with that in the negative control, which may be due to an increase in antibody expression over time. Furthermore, in the rabbit disease model, subretinal injection was chosen because chronic intravitreal injection of AAV must bypass the inner limiting membrane (ILM). In the above mouse experiments, especially in the newborn mice used for OIR modeling, subretinal injection was difficult because of the small size of the eyeball, so only vitreous cavity injection was chosen. The ILM is a typical basement membrane that forms the vitreoretinal junction and acts as a biological barrier to intravitreal injected capsids.<sup>45</sup> Primates have a more impenetrable ILM than

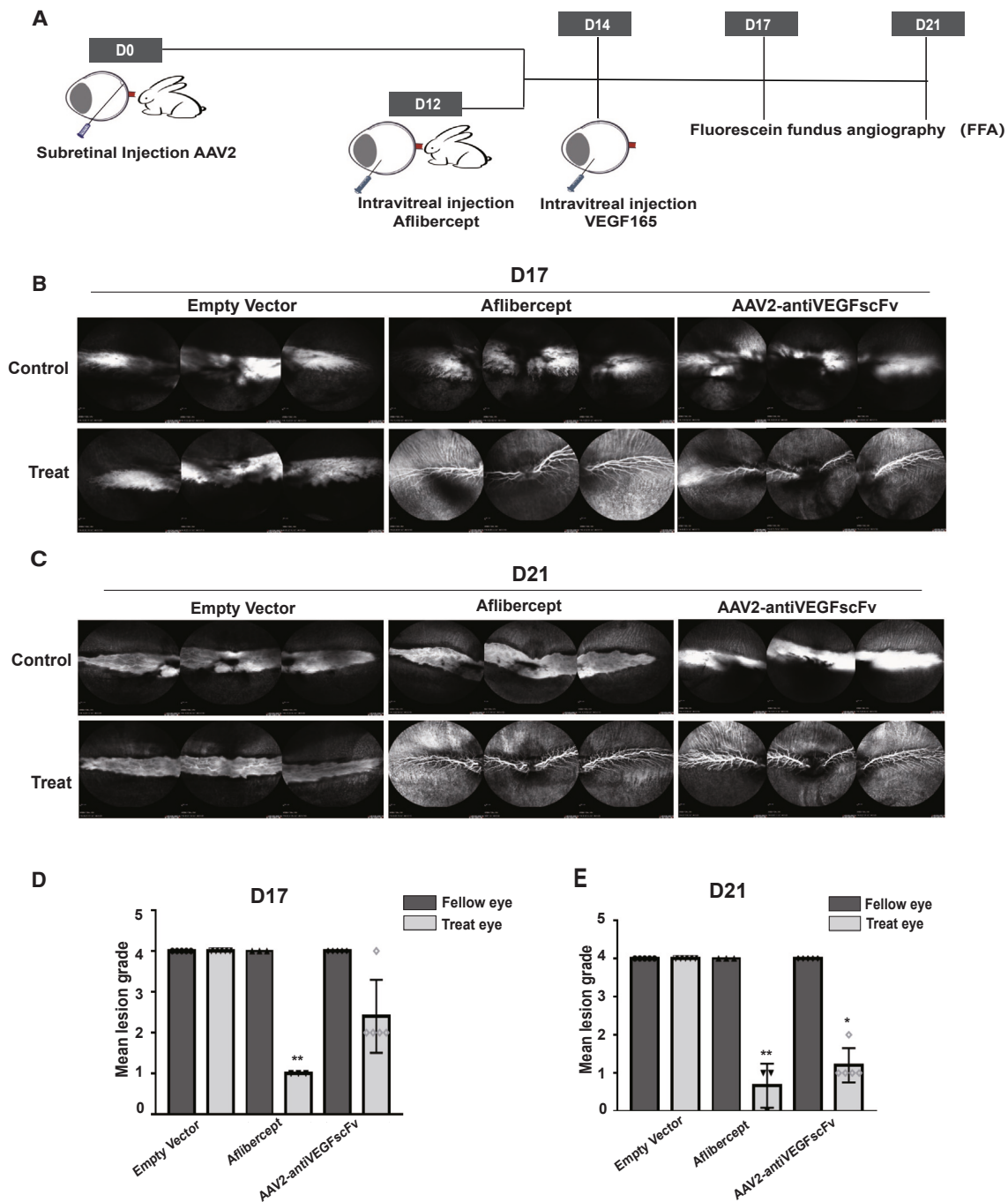
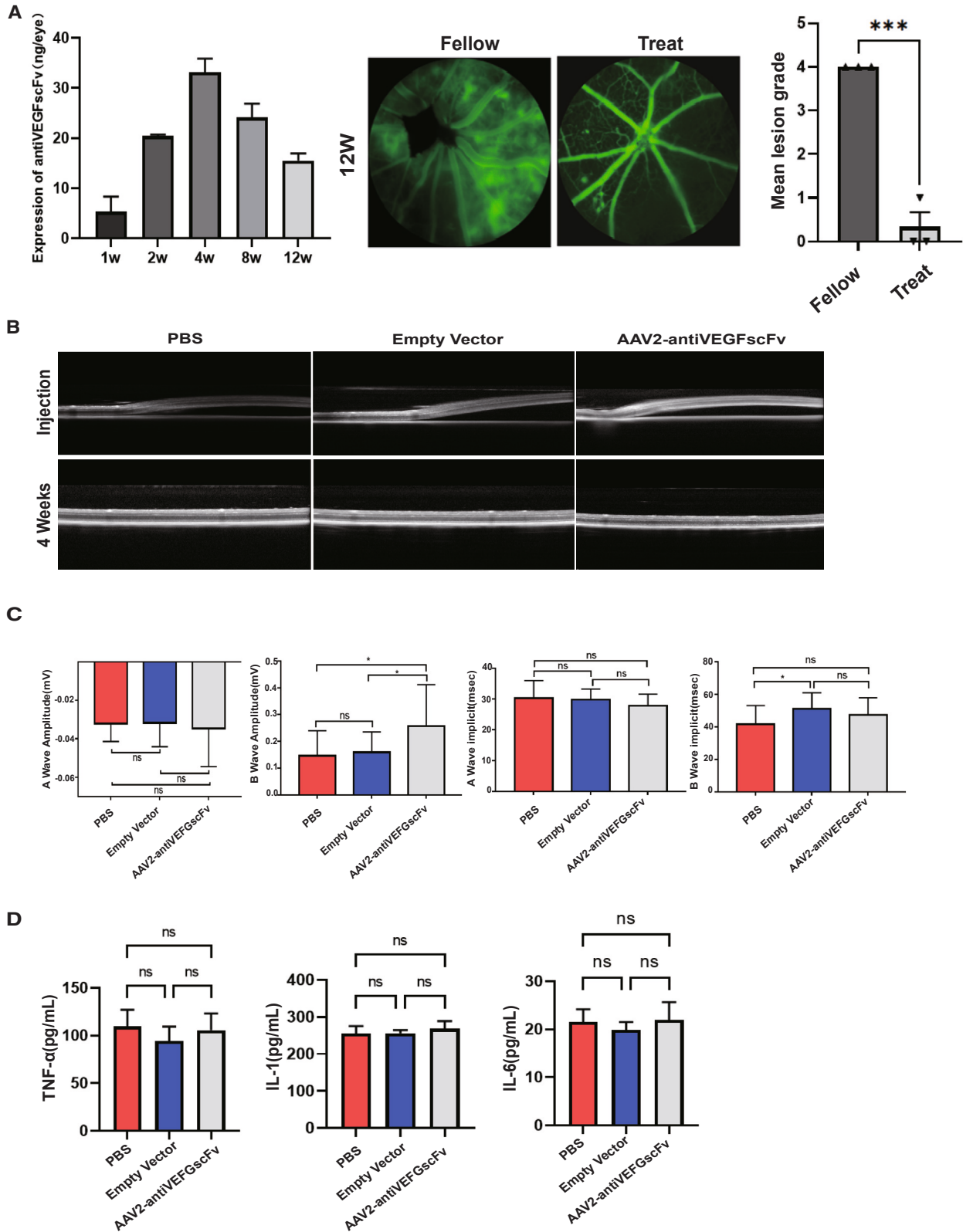


**Figure 6. AAV2-antiVEGFscFv blocks vascular leakage in a VEGF-induced rabbit NV model**

(A) The experimental flowchart. Dutch belted rabbits, male, 3–6 months old. (B) Day 17 fluorescein fundus angiography (FFA) images in groups of empty vector, aflibercept, and AAV2-antiVEGFscFv, including treatment eye and contralateral eye. Each column represents one animal at various times of follow-up. Similar results are seen in the other animals within each group. (C) Quantitative statistical graph of (B). (D) Day 21 FFA images in groups, similar results are seen in the other animals within each group. (E) Quantitative statistical graph of (D). One-way ANOVA was used for statistical analysis, and data are mean  $\pm$  standard error. \*\* $p < 0.01$ . Empty vector and AAV2-antiVEGFscFv groups,  $n = 5$ ; aflibercept group,  $n = 3$ .



(legend on next page)

rodents.<sup>46</sup> Subretinal injections resulted in better retinal gene transfer than intravitreal injection.<sup>47</sup> In addition, this selection can provide a certain degree of reference for the dosage and volume of the drug in subsequent primate experiments.

The results presented here represent the first instance of preclinical evidence demonstrating robust expression and efficacy of AAV2-antiVEGFscFv at a dose that was well tolerated in mice and did not lead to the evidence of ocular inflammation. This study suggests that AAV2-antiVEGFscFv may be a potential treatment strategy for NV, laying the foundation for subsequent preclinical studies in non-human primates and providing strong support for its clinical application.

## MATERIALS AND METHODS

### Animals

All animals underwent experimentation in compliance with standards of China Medical University Animal Ethics Committee (CMU2021552).

### OIR mice

The OIR model was carried out in C57BL/6J mice as previously described by Connor et al.<sup>42</sup> Wild-type C57BL/6J mice were purchased from Beijing Viton Lever. Newborn mice were housed in a room air (21% O<sub>2</sub>) with their nursing mothers from birth to P7. They were housed with their mothers in a 75% O<sub>2</sub> hyperoxia environment from P7 to P12, leading to vaso-obliteration in several retinal areas. Then, newborn mice were returned to a room air and received intravitreal injection at P12. The relative hypoxia over the subsequent 5 days promotes excess VEGF production and leads to tufts of new blood vessels characteristic of the pathological RNV form on the inner surface of the retina at P17. All the OIR mice were randomly divided into four groups, and each group included five mice.

### Intravitreal injection

At P12, the OIR mice were received intravitreal injection. First, the mice were anesthetized with 1% pentobarbital sodium (50 mg/kg), and compound tropicamide drops were administered on the corneal surface. Next, 1  $\mu$ L empty vector ( $2.5 \times 10^8$  GC), aflibercept (40  $\mu$ g), or AAV-antiVEGFscFv ( $2.5 \times 10^8$  GC) was injected into the vitreous. A 33G beveled needle affixed to a Hamilton syringe (2.5  $\mu$ L; Hamilton, Reno, NV) was used to puncture into the vitreous cavity medially at the corneoscleral rim, and then slowly pushed in, under a stereomicroscope to avoid lens injury. Immediately after the syringe was withdrawn, levofloxacin hydrochloride gel was applied to the inlet port to prevent drug leakage and infection after the operation.

### Tet/opsin/VEGF mice and treatment

Double-transgenic mice (*Tet/opsin/VEGF mice*) induced to express VEGF in photoreceptors were purchased from Southern Model Or-

ganisms, were in a C57BL/6 background, and were genotyped to confirm the presence of the transgene prior to use in the experiments. The virus is injected through the vitreous cavity in the fourth week after birth. See [intravitreal injection](#) for specific injection methods. In addition, 2  $\mu$ L PBS, empty vector ( $5 \times 10^8$  GC), or AAV-antiVEGFscFv ( $5 \times 10^8$  GC) was injected into the vitreous. Doxycycline was added to the drinking water for induction at a concentration of 2 mg/mL, starting 2 weeks after vitreous injection of the virus. All mice were randomly divided into three groups, and each group included five mice.

### VEGF-induced rabbit and treatment

Dutch black-banded rabbits were purchased from Pizhou Oriental Breeding. Animals in all groups were molded by bilateral vitreous cavity injection of human-derived VEGFA<sub>165</sub> (dose of 1.8  $\mu$ g/eye, 50  $\mu$ L/eye). Under an ophthalmology-specific surgical microscope (M620; Leica), the corneoscleral rim was punctured medially with a 30G disposable injection needle, and a microinjector with a 35G flat needle was used to enter along the puncture and bypass the lens to reach the vitreous, where the syringe reached the vitreous cavity and was slowly pushed in. Immediately after withdrawing the syringe, the injection port was compressed for 5 s with a swab with iodophor. Empty vector and AAV2-antiVEGFscFv group were injected unilaterally in the subretinal cavity. The previous steps were the same as for vitreous cavity injection, then the needle was gradually advanced into the subretinal space and slowly pushed out. The aflibercept group was injected unilaterally into the vitreous cavity (2 mg/eye, 50  $\mu$ L/eye) 2 days prior to entry (D12). FFA images were taken at D17 and D21. All animals were randomly divided into three groups. The empty vector group and AAV-antiVEGFscFv group included five animals each, and the aflibercept group included three animals.

### Plasmids

AAV2-antiVEGFscFv is a non-replicative AAV2 vector containing a gene cassette encoding a humanized monoclonal antigen-binding fragment that binds and represses human VEGF flanked by an AAV2 inverted terminal repeat (ITR) sequence. Expression of the heavy and light chains is controlled by the CBA promoter, which consists of the chicken  $\beta$ -actin promoter and CMV enhancer, the chicken  $\beta$ -actin intron, and the rabbit  $\beta$ -bead protein poly(A) signal. The expressed protein products were similar but not identical to brolicuzumab. The AAV2 rep/cap plasmid, and pAD helper plasmid for recombinant AAV2 vector production were obtained from Addgene (Cambridge, MA).

### Production of recombinant AAV2 viral vectors

Recombinant AAV2 full particles expressing antiVEGFscFv were produced using triple transfection in HEK293T cells, as previously described.<sup>8</sup> In brief, the transgene plasmid pAAV2-antiVEGFscFv,

## Figure 7. Long-term expression and safety assessment of AAV2-antiVEGFscFv in eyes

(A) Long-term gene expression of antiVEGFscFv. n = 3. (B) OCT images taken on the day of completion of subretinal injection and one month later. n = 16. (C) Statistical results of amplitudes of ERG A wave and B wave in mice examined one month after administration. n = 16. (D) The expression of inflammatory factors in the retinas of mice. n = 3. One-way ANOVA was used for statistical analysis, and data are mean  $\pm$  standard error. \*p < 0.05; ns, not significant.

the AAV helper plasmid containing Rep and Cap genes, and the adenoviral helper plasmid pAD were co-transfected into HEK293T cells. HEK293T cells were collected and lysed 72 h post-transfection. The supernatant was then subjected to a cesium chloride gradient ultracentrifugation.

#### Cell culture

HUVECs were purchased from ScienCell Research Laboratories (San Diego, CA) and cultured in endothelial cell medium (ScienCell Research Laboratories) supplemented with 5% fetal bovine serum (FBS) (ScienCell Research Laboratories) and 1% endothelial cell growth supplement (ScienCell Research Laboratories) in a humidified incubator containing 5% CO<sub>2</sub> in a humidified atmosphere at 37°C incubator to grow HEK293T cells in DMEM + 10% FBS. A humidified incubator at 37°C and 5% CO<sub>2</sub> was used to culture 293T cells and HUVECs.

#### *In vitro* testing of AAV2-antiVEGFscFv

HEK293T cells were inoculated into 24-well plates at a density of  $5 \times 10^5$  cells/well in 200 mL DMEM containing 10% FBS and 100 U/mL penicillin/streptomycin. Twelve hours later, under a microscope, when the cell density grew to 80%, the cells were transduced with AAV2-antiVEGFscFv or empty vector virus configured with multiplicities of infection (MOIs) of 1:5,000, 1:50,000, and 1:500,000, respectively. The cells and supernatant were collected after 48 h and used for western blot and ELISA to determine protein expression.

#### Western blot

Proteins were extracted from cells and supernatants obtained by *in vitro* transfection of AAV, cells were extracted using NP40 lysate, and equal amounts of proteins were electrophoresed on 12% SDS-polyacrylamide gels. The proteins were transferred to polyvinylidene difluoride membranes (Merck Millipore) and then closed with 5% skim milk powder solution containing Tween 20 (TBST; pH 7.5) diluted in TBST at (RT) for 1 h. After dilution with anti-anti-VEGFscFv specific antibody (Zhongding Biologics) 1:5,000 or anti-actin antibody (ab197345; Abcam). The membrane was washed 3 times with  $1 \times$  TBST for 10 min each time to completely wash out the residual primary antibody, and the secondary antibody horseradish peroxidase (HRP)-conjugated Affinipure Goat Anti-Rabbit IgG(H+L) (SA00001-2; Proteintech) was then added, diluted 1:5,000 and incubated for 60 min at RT. The membrane was washed 5 times for 5 min each time and then imaged in a pre-cooled chemiluminescence instrument.

#### ELISA

Antibody expression and ability to bind VEGF was analyzed using ELISA by coating 96-well ELISA plates (Fisher, Loughborough, UK) with  $1 \mu\text{g/mL}$  hVEGF (Z02689; Kingsley) and incubated overnight at 4°C. Plates were then closed by incubation in 2% BSA at 37°C for 1 h. Culture supernatant was placed in triplicate in the wells and incubated at 37°C for 2 h. Anti-antiVEGFscFv-specific antibody diluted 1:5,000 in blocking buffer was used, with incubation for 2 h at RT. Incubation was performed for 1 h at RT with HRP-conjugated

Affinipure Goat Anti-Rabbit IgG(H+L) diluted 1:5,000 in blocking buffer. After each of the above steps, the plate was washed 5 times with PBS + 0.05% Tween 20. After adding HRP substrate and developing color in the dark at 37°C, the reaction is terminated with 3,3',5,5'-tetramethylbenzidine (TMB) (Sigma-Aldrich, St. Louis, MO) at RT in the dark for 30 min, after which 50  $\mu\text{L}$  stop solution (2NH<sub>2</sub>SO<sub>4</sub>) was added to each well, and the plate was read at 450 nm. TNF- $\alpha$  (RX203097M; Ruixin Biotech), IL-1 (RX203076M; Ruixin Biotech), and IL-6 (RX203049M; Ruixin Biotech) were detected according to the manufacturer's instructions.

#### Eye tissue homogenization

The eyeballs were removed immediately after death, and individual eyeball tissues were rinsed with pre-cooled PBS (0.01 M, pH 7.4) to remove any residual blood and weighed. After weighing, the slices were processed, and 200  $\mu\text{L}$  NP40 was added. Slices were then pressed until the tissue is fully dissolved. Finally, the homogenate was centrifuged at  $5,000 \times g$  for 5–10 min, and the supernatant was diluted with PBS for subsequent detection using ELISA.

#### Cell migration

The migration ability of HUVECs was measured in the wound healing assay. First, 6-well plates of  $2 \times 10^6$  cells/mL HUVECs were prepared, and the cell density reached 70%–80% when the serum-free medium was changed to add empty vector or AAV2-antiVEGFscFv (MOI = 1:100,000) to infect the cells respectively for 48 h, and then the supernatant of clean medium was collected. Cells were created by scratching using a sterile gun tip, then recombinant human VEGF<sub>165</sub> (50 ng/mL) or brolucizumab (100 ng/mL) was added to the collected supernatants of different subgroups (as indicated in the results), mixed well, and added to the wells. Cells were incubated at 37°C for 0–24 h to observe the scratch healing rate. Cell images were obtained immediately after scratching and again by inverted fluorescence microscopy (Olympus) at four time points (0, 6, 12, and 24 h) after cells migrated to the scratched area. For each image, the wound area was quantified using ImageJ version 1.46r (NIH), and the scratch closure rate was determined by normalizing it to the original wound area. All experiments were performed in triplicate.

#### Cell proliferation

Logarithmic growth phase HUVECs were taken, digested with 0.25% trypsin, and resuspended in ECM medium without FBS. The cell suspension density was adjusted to  $1 \times 10^5$  cells/mL, and 100  $\mu\text{L}$  per well was inoculated in 96-well plates. Incubation was performed with ECM medium without FBS in a 5% CO<sub>2</sub>, 37°C incubator, with starvation for 24 h. AAV2-antiVEGFscFv, empty vector with ECM without FBS were diluted, and the MOI was set to 1:500,000, 1:50,000, 1:5,000, respectively; the original cell culture medium was removed, and 100  $\mu\text{L}$  ECM medium without FBS was added as a blank control group, 100  $\mu\text{L}$  VEGF<sub>165</sub> (50 ng/mL) was added as a positive control group, and brolucizumab (ATAD00374; Atagenix) was added as a drug intervention group at concentrations of 2  $\mu\text{g/mL}$ , 200 ng/mL, and 20 ng/mL, respectively, and 3 parallel wells were set up for each group and incubated in a 5% CO<sub>2</sub>, 37°C

incubator for another 48 h. CCK8 (C6005; NCM Biotech) 10  $\mu$ L was added to each well, and the incubation was continued for 2 h with 5% CO<sub>2</sub> in 37°C incubators. The optical density (OD) value of each well was measured at 450 nm with an enzyme marker and the test was repeated three times.

#### Retinal IB4 staining

Retinas were immersed in 5% Triton X-100 and incubated overnight at 4°C. At the end of the incubation, the retinas were washed three times with PBS, and immediately 500  $\mu$ L lectin solution (I21412; Invitrogen) was added, wrapped in aluminum foil to protect from light, and shaken overnight at RT. At the end of staining, the retinas were washed again three times with PBS. The stained retina was placed on a slide, and four incisions were made from the center to the edge of the retina, each at an angle of 90°C. A drop of sealer was added to the coverslip, and the retina was then covered for fixation. Using a Nikon C2 laser confocal microscope at 10 $\times$  magnification, the whole retinal pavement was scanned, and the complete image was synthesized.

#### FFA and OCT

Animals were placed on a Micron III camera (Phoenix Labs). The animal was placed on a heated platform. The retina is focused and the camera lens objective is pointed at the eye. A 0.3 mL of 2% fluorescein (Centaur Services) was injected intraperitoneally. Early (30 s) and late (3 min) FFA images were captured for each eye using a version of Streampix (Phoenix Labs). OCT images were subsequently captured and analyzed using OCT Explore.

#### H&E staining and IHC

Mice were euthanized, eyes were removed and frozen, and 10  $\mu$ m serial sections were cut. Sections were partially post-fixed in 4% paraformaldehyde, stained with H&E, and examined using light microscopy to determine the presence and extent of exudative retinal detachment.

Immunohistochemical sections were blocked with 2% BSA and then washed with PBS, followed by incubation with rabbit anti-IL-1 $\beta$  (YT5201; Immunoway), rabbit anti-IL-6 (YT5348; Immunoway), or rabbit anti-TNF- $\alpha$  (YT4689; Immunoway). After that, the slides were incubated with secondary antibody HRP-conjugated Affinipure Goat Anti-Rabbit IgG(H+L) and photographed under the microscope.

#### Immunofluorescence

Paraffin sections of eye tissue were taken, closed with 2% BSA, and washed in PBS, followed by incubation with rabbit anti-anti-VEGFscFv and anti-F4/80 (71299; Cell Signaling Technology). After that, the slides were incubated with CY3 fluorescent labeled goat anti-rabbit IgG (GB21303; Servicebio). After incubation, nuclei were restained with DAPI solution, and fluorescent images were collected using microscopy for analysis.

#### ERG

The mice were placed in a dark room overnight (at least 12 h) prior to the examination. After anesthesia, the mice were fixed on the oper-

ating table, pupil-dilating drops were added, electrodes were fitted, and the ERG was measured and recorded using a Diagnosys Celeris small animal electrophysiologist.

#### CBA

Wild-type mice blood was collected from a peripheral vein after ocular injections of AAVs. The blood sample was centrifuged at 800  $\times$  g for 10 min, and the serum (supernatant) was transferred into a separate Eppendorf tube and stored at -80°C until for CBA detection.

IFN- $\gamma$  (558296; BD Biosciences), TNF (558299; BD Biosciences), and IL-2 (558297; BD Biosciences) were assessed using BD CBA Mouse/Rat Soluble Protein Master Buffer Kit (558266; BD Biosciences), according to the manufacturer's instructions. Data were captured using a BD Accuri C6 flow cytometer (BD Biosciences) and analyzed using FCAP Array version 3 (BD Biosciences).

#### Statistical analysis

Statistical analysis was performed using GraphPad Prism 7.0 software. One-way ANOVA was used for univariate analysis. *p* values <0.05 were considered to indicate statistical significance.

#### DATA AND CODE AVAILABILITY

The data used and/or analyzed in the present study are available from the corresponding author on reasonable request.

#### ACKNOWLEDGMENTS

We thank Drs. Fangkun Zhao and Jun Kong for their help and knowledge of the experimental design and methods. This work is supported by the National Natural Science Foundation of China (grant 82070826).

#### AUTHOR CONTRIBUTIONS

Conceptualization, methodology, visualization, and project administration, N.H., X.X., Y.L., and G.L.; investigation, N.H., X.X., Y.L., and G.L.; software and data curation, N.H. and X.X.; formal analysis, N.H. and X.X.; writing – original draft, N.H. and X.X.; writing, review & editing, N.H., X.X., Y.L., and G.L.; resources – Y.L. and G.L.; supervision, Y.L. and G.L.; funding acquisition, Y.L. and G.L.

#### DECLARATION OF INTERESTS

The authors declare no competing interests.

#### REFERENCES

- Hou, X.W., Wang, Y., Ke, C.F., Li, M.Y., and Pan, C.W. (2022). Metabolomics and Biomarkers in Retinal and Choroidal Vascular Diseases. *Metabolites* 12, 814. <https://doi.org/10.3390/metabo12090814>.
- Honasoge, A., Nudleman, E., Smith, M., and Rajagopal, R. (2019). Emerging Insights and Interventions for Diabetic Retinopathy. *Curr. Diabetes Rep.* 19, 100. <https://doi.org/10.1007/s11892-019-1218-2>.
- Ferrara, N. (2016). VEGF and Intraocular Neovascularization: From Discovery to Therapy. *Transl. Vis. Sci. Technol.* 5, 10. <https://doi.org/10.1167/tvst.5.2.10>.

4. Wang, J.H., Lin, F.L., Chen, J., Zhu, L., Chuang, Y.F., Tu, L., Ma, C., Ling, D., Hewitt, A.W., Tseng, C.L., et al. (2023). TAK1 blockade as a therapy for retinal neovascularization. *Pharmacol. Res.* 187, 106617. <https://doi.org/10.1016/j.phrs.2022.106617>.
5. Comparison of Age-related Macular Degeneration Treatments Trials CATT Research Group, Maguire, M.G., Martin, D.F., Ying, G.S., Jaffe, G.J., Daniel, E., Grunwald, J.E., Toth, C.A., Ferris, F.L., 3rd, and Fine, S.L. (2016). Five-Year Outcomes with Anti-Vascular Endothelial Growth Factor Treatment of Neovascular Age-Related Macular Degeneration: The Comparison of Age-Related Macular Degeneration Treatments Trials. *Ophthalmology* 123, 1751–1761. <https://doi.org/10.1016/j.ophtha.2016.03.045>.
6. Dakin, H.A., Wordsworth, S., Rogers, C.A., Abangma, G., Raftery, J., Harding, S.P., Lotery, A.J., Downes, S.M., Chakravarthy, U., and Reeves, B.C.; IVAN Study Investigators (2014). Cost-effectiveness of ranibizumab and bevacizumab for age-related macular degeneration: 2-year findings from the IVAN randomised trial. *BMJ Open* 4, e005094. <https://doi.org/10.1136/bmjopen-2014-005094>.
7. Kelly, P.J., Lin, Y.B., Yu, A.Y., Alexander, B.M., Hacker, F., Marcus, K.J., and Weiss, S.E. (2012). Stereotactic irradiation of the postoperative resection cavity for brain metastasis: a frameless linear accelerator-based case series and review of the technique. *Int. J. Radiat. Oncol. Biol. Phys.* 82, 95–101. <https://doi.org/10.1016/j.ijrobp.2010.10.043>.
8. Meng, Y., Sun, D., Qin, Y., Dong, X., Luo, G., and Liu, Y. (2021). Cell-penetrating peptides enhance the transduction of adeno-associated virus serotype 9 in the central nervous system. *Mol. Ther. Methods Clin. Dev.* 21, 28–41. <https://doi.org/10.1016/j.omtm.2021.02.019>.
9. Khanani, A.M., Thomas, M.J., Aziz, A.A., Weng, C.Y., Danzig, C.J., Yiu, G., Kiss, S., Waheed, N.K., and Kaiser, P.K. (2022). Review of gene therapies for age-related macular degeneration. *Eye* 36, 303–311. <https://doi.org/10.1038/s41433-021-01842-1>.
10. Wykoff, C.C., Abreu, F., Adams, A.P., Basu, K., Eichenbaum, D.A., Haskova, Z., Lin, H., Loewenstein, A., Mohan, S., Pearce, I.A., et al. (2022). Efficacy, durability, and safety of intravitreal faricimab with extended dosing up to every 16 weeks in patients with diabetic macular oedema (YOSEMITE and RHINE): two randomised, double-masked, phase 3 trials. *Lancet* 399, 741–755. [https://doi.org/10.1016/s0140-6736\(22\)00018-6](https://doi.org/10.1016/s0140-6736(22)00018-6).
11. Kiss, S., Oresic Bender, K., Grishanin, R.N., Hanna, K.M., Nieves, J.D., Sharma, P., Nguyen, A.T., Rosario, R.J., Greengard, J.S., Gelfman, C.M., and Gasmi, M. (2021). Long-Term Safety Evaluation of Continuous Intraocular Delivery of Aflibercept by the Intravitreal Gene Therapy Candidate ADVN-022 in Nonhuman Primates. *Transl. Vis. Sci. Technol.* 10, 34. <https://doi.org/10.1167/tvst.10.1.34>.
12. Liu, Y., Fortmann, S.D., Shen, J., Wielechowski, E., Tretiakova, A., Yoo, S., Kozarsky, K., Wang, J., Wilson, J.M., and Campochiaro, P.A. (2018). AAV8-antiVEGF Fab Ocular Gene Transfer for Neovascular Age-Related Macular Degeneration. *Mol. Ther.* 26, 542–549. <https://doi.org/10.1016/j.ymthe.2017.12.002>.
13. Huang, H., Parlier, R., Shen, J.K., Luttly, G.A., and Vinore, S.A. (2013). VEGF receptor blockade markedly reduces retinal microglia/macrophage infiltration into laser-induced CNV. *PLoS One* 8, e71808. <https://doi.org/10.1371/journal.pone.0071808>.
14. Gao, S., Li, C., Zhu, Y., Wang, Y., Sui, A., Zhong, Y., Xie, B., and Shen, X. (2017). PEDF mediates pathological neovascularization by regulating macrophage recruitment and polarization in the mouse model of oxygen-induced retinopathy. *Sci. Rep.* 7, 42846. <https://doi.org/10.1038/srep42846>.
15. Yang, S., Li, T., Jia, H., Gao, M., Li, Y., Wan, X., Huang, Z., Li, M., Zhai, Y., Li, X., et al. (2022). Targeting C3b/C4b and VEGF with a bispecific fusion protein optimized for neovascular age-related macular degeneration therapy. *Sci. Transl. Med.* 14, eabj2177. <https://doi.org/10.1126/scitranslmed.abj2177>.
16. Chandler, L.C., McClements, M.E., Yusuf, I.H., Martinez-Fernandez de la Camara, C., MacLaren, R.E., and Xue, K. (2021). Characterizing the cellular immune response to subretinal AAV gene therapy in the murine retina. *Mol. Ther. Methods Clin. Dev.* 22, 52–65. <https://doi.org/10.1016/j.omtm.2021.05.011>.
17. Qiu, G., Stewart, J.M., Satta, S., Freda, R., Lee, S., Guven, D., de Juan, E., Jr., and Varner, S.E. (2006). A new model of experimental subretinal neovascularization in the rabbit. *Exp. Eye Res.* 83, 141–152. <https://doi.org/10.1016/j.exer.2005.11.014>.
18. Bucher, K., Rodríguez-Bocanegra, E., Daultebekov, D., and Fischer, M.D. (2021). Immune responses to retinal gene therapy using adeno-associated viral vectors - Implications for treatment success and safety. *Prog. Retin. Eye Res.* 83, 100915. <https://doi.org/10.1016/j.preteyeres.2020.100915>.
19. Grishanin, R., Vuilleminot, B., Sharma, P., Keravala, A., Greengard, J., Gelfman, C., Blumenkrantz, M., Lawrence, M., Hu, W., Kiss, S., and Gasmi, M. (2019). Preclinical Evaluation of ADVN-022, a Novel Gene Therapy Approach to Treating Wet Age-Related Macular Degeneration. *Mol. Ther.* 27, 118–129. <https://doi.org/10.1016/j.ymthe.2018.11.003>.
20. Bayramoglu, S.E., and Sayin, N. (2022). Inter-eye comparison of retinal vascular growth rate and angiographic findings following unilateral bevacizumab treatment. *Eur. J. Ophthalmol.* 32, 1430–1440. <https://doi.org/10.1177/11206721211064019>.
21. Avery, R.L., Castellarin, A.A., Steinle, N.C., Dhoot, D.S., Pieramici, D.J., See, R., Couvillion, S., Nasir, M.A., Rabena, M.D., Maia, M., et al. (2017). SYSTEMIC PHARMACOKINETICS AND PHARMACODYNAMICS OF INTRAVITREAL AFLIBERCEPT, BEVACIZUMAB, AND RANIBIZUMAB. *Retina* 37, 1847–1858. <https://doi.org/10.1097/iae.0000000000001493>.
22. Mitchell, P., Holz, F.G., Hykin, P., Midena, E., Souied, E., Allmeier, H., Lambrou, G., Schmelzer, T., and Wolf, S.; ARIES study investigators (2021). EFFICACY AND SAFETY OF INTRAVITREAL AFLIBERCEPT USING A TREAT-AND-EXTEND REGIMEN FOR NEOVASCULAR AGE-RELATED MACULAR DEGENERATION: THE ARIES STUDY: A RANDOMIZED CLINICAL TRIAL. *Retina* 41, 1911–1920. <https://doi.org/10.1097/iae.0000000000003128>.
23. Fogli, S., Del Re, M., Rofi, E., Posarelli, C., Figus, M., and Danesi, R. (2018). Clinical pharmacology of intravitreal anti-VEGF drugs. *Eye (Lond)* 32, 1010–1020. <https://doi.org/10.1038/s41433-018-0021-7>.
24. Motevassel, T., Mohammadi, S., Abdi, F., and Freeman, W.R. (2021). Side Effects of Brolicizumab. *J. Ophthalmic Vis. Res.* 16, 670–675. <https://doi.org/10.18502/jovr.v16i4.9757>.
25. Tadayoni, R., Sararols, L., Weissgerber, G., Verma, R., Clemens, A., and Holz, F.G. (2021). Brolicizumab: A Newly Developed Anti-VEGF Molecule for the Treatment of Neovascular Age-Related Macular Degeneration. *Ophthalmologica* 244, 93–101. <https://doi.org/10.1159/000513048>.
26. Tiller, K.E., and Tessier, P.M. (2015). Advances in Antibody Design. *Annu. Rev. Biomed. Eng.* 17, 191–216. <https://doi.org/10.1146/annurev-bioeng-071114-040733>.
27. Murinello, S., Mullins, R.F., Lotery, A.J., Perry, V.H., and Teeling, J.L. (2014). Fcy receptor upregulation is associated with immune complex inflammation in the mouse retina and early age-related macular degeneration. *Invest. Ophthalmol. Vis. Sci.* 55, 247–258. <https://doi.org/10.1167/iovs.13-11821>.
28. Hughes, C.P., O'Flynn, N.M.J., Gatherer, M., McClements, M.E., Scott, J.A., MacLaren, R.E., Goverdhan, S., Glennie, M.J., and Lotery, A.J. (2019). AAV2/8 Anti-angiogenic Gene Therapy Using Single-Chain Antibodies Inhibits Murine Choroidal Neovascularization. *Molecular therapy. Mol. Ther. Methods Clin. Dev.* 13, 86–98. <https://doi.org/10.1016/j.omtm.2018.11.005>.
29. Bainbridge, J.W.B., Mehat, M.S., Sundaram, V., Robbie, S.J., Barker, S.E., Ripamonti, C., Georgiadis, A., Mowat, F.M., Beattie, S.G., Gardner, P.J., et al. (2015). Long-term effect of gene therapy on Leber's congenital amaurosis. *N. Engl. J. Med.* 372, 1887–1897. <https://doi.org/10.1056/NEJMoa1414221>.
30. Boyd, R.F., Boye, S.L., Conlon, T.J., Erger, K.E., Sledge, D.G., Langohr, I.M., Hauswirth, W.W., Komáromy, A.M., Boye, S.E., Petersen-Jones, S.M., and Bartoe, J.T. (2016). Reduced retinal transduction and enhanced transgene-directed immunogenicity with intravitreal delivery of rAAV following posterior vitrectomy in dogs. *Gene Ther.* 23, 548–556. <https://doi.org/10.1038/gt.2016.31>.
31. Srivastava, A. (2016). In vivo tissue-tropism of adeno-associated viral vectors. *Curr. Opin. Virol.* 21, 75–80. <https://doi.org/10.1016/j.coviro.2016.08.003>.
32. Mendell, J.R., Al-Zaidy, S.A., Rodino-Klapac, L.R., Goodspeed, K., Gray, S.J., Kay, C.N., Boye, S.L., Boye, S.E., George, L.A., Salabarria, S., et al. (2021). Current Clinical Applications of In Vivo Gene Therapy with AAVs. *Mol. Ther.* 29, 464–488. <https://doi.org/10.1016/j.ymthe.2020.12.007>.
33. Maguire, A.M., Bennett, J., Aleman, E.M., Leroy, B.P., and Aleman, T.S. (2021). Clinical Perspective: Treating RPE65-Associated Retinal Dystrophy. *Mol. Ther.* 29, 442–463. <https://doi.org/10.1016/j.ymthe.2020.11.029>.
34. Sprague, A.H., and Khalil, R.A. (2009). Inflammatory cytokines in vascular dysfunction and vascular disease. *Biochem. Pharmacol.* 78, 539–552. <https://doi.org/10.1016/j.bcp.2009.04.029>.
35. Li, W., Asokan, A., Wu, Z., Van Dyke, T., DiPrimio, N., Johnson, J.S., Govindaswamy, L., Agbandje-McKenna, M., Leichter, S., Eugene Redmond, D., Jr., et al. (2008).

- Engineering and Selection of Shuffled AAV Genomes: A New Strategy for Producing Targeted Biological Nanoparticles. *Mol. Ther.* 16, 1252–1260. <https://doi.org/10.1038/mt.2008.100>.
36. Reichel, F.F., Seitz, I., Wozar, F., Dimopoulos, S., Jung, R., Kempf, M., Kohl, S., Kortüm, F.C., Ott, S., Pohl, L., et al. (2023). Development of retinal atrophy after sub-retinal gene therapy with voretigene neparvec. *Br. J. Ophthalmol.* 107, 1331–1335. <https://doi.org/10.1136/bjophthalmol-2021-321023>.
  37. Horiuchi, M., Hinderer, C.J., Shankle, H.N., Hayashi, P.M., Chichester, J.A., Kissel, C., Bell, P., Dyer, C., and Wilson, J.M. (2023). Neonatal Fc Receptor Inhibition Enables Adeno-Associated Virus Gene Therapy Despite Pre-Existing Humoral Immunity. *Hum. Gene Ther.* 34, 1022–1032. <https://doi.org/10.1089/hum.2022.216>.
  38. Seitz, I.P., Michalakos, S., Wilhelm, B., Reichel, F.F., Ochakovski, G.A., Zrenner, E., Ueffing, M., Biel, M., Wissinger, B., Bartz-Schmidt, K.U., et al. (2017). Superior Retinal Gene Transfer and Biodistribution Profile of Subretinal Versus Intravitreal Delivery of AAV8 in Nonhuman Primates. *Invest. Ophthalmol. Vis. Sci.* 58, 5792–5801. <https://doi.org/10.1167/iovs.17-22473>.
  39. Kotterman, M.A., Yin, L., Strazzeri, J.M., Flannery, J.G., Merigan, W.H., and Schaffer, D.V. (2015). Antibody neutralization poses a barrier to intravitreal adeno-associated viral vector gene delivery to non-human primates. *Gene Ther.* 22, 116–126. <https://doi.org/10.1038/gt.2014.115>.
  40. Lambert, V., Lecomte, J., Hansen, S., Blacher, S., Gonzalez, M.L.A., Struman, I., Sounni, N.E., Rozet, E., de Tullio, P., Foidart, J.M., et al. (2013). Laser-induced choroidal neovascularization model to study age-related macular degeneration in mice. *Nat. Protoc.* 8, 2197–2211. <https://doi.org/10.1038/nprot.2013.135>.
  41. Tang, X., Cui, K., Lu, X., Wu, P., Yu, S., Yang, B., Xu, Y., and Liang, X. (2022). A Novel Hypoxia-inducible Factor 1 $\alpha$  Inhibitor KC7F2 Attenuates Oxygen-induced Retinal Neovascularization. *Invest. Ophthalmol. Vis. Sci.* 63, 13. <https://doi.org/10.1167/iovs.63.6.13>.
  42. Connor, K.M., Krah, N.M., Dennison, R.J., Aderman, C.M., Chen, J., Guerin, K.I., Sapielha, P., Stahl, A., Willett, K.L., and Smith, L.E.H. (2009). Quantification of oxygen-induced retinopathy in the mouse: a model of vessel loss, vessel regrowth and pathological angiogenesis. *Nat. Protoc.* 4, 1565–1573. <https://doi.org/10.1038/nprot.2009.187>.
  43. Ohno-Matsui, K., Hirose, A., Yamamoto, S., Saikia, J., Okamoto, N., Gehlbach, P., Duh, E.J., Hackett, S., Chang, M., Bok, D., et al. (2002). Inducible expression of vascular endothelial growth factor in adult mice causes severe proliferative retinopathy and retinal detachment. *Am. J. Pathol.* 160, 711–719. [https://doi.org/10.1016/s0002-9440\(10\)64891-2](https://doi.org/10.1016/s0002-9440(10)64891-2).
  44. Grossniklaus, H.E., Kang, S.J., and Berglin, L. (2010). Animal models of choroidal and retinal neovascularization. *Prog. Retin. Eye Res.* 29, 500–519. <https://doi.org/10.1016/j.preteyeres.2010.05.003>.
  45. Dalkara, D., Kolstad, K.D., Caporale, N., Visel, M., Klimczak, R.R., Schaffer, D.V., and Flannery, J.G. (2009). Inner limiting membrane barriers to AAV-mediated retinal transduction from the vitreous. *Mol. Ther.* 17, 2096–2102. <https://doi.org/10.1038/mt.2009.181>.
  46. Matsumoto, B., Blanks, J.C., and Ryan, S.J. (1984). Topographic variations in the rabbit and primate internal limiting membrane. *Invest. Ophthalmol. Vis. Sci.* 25, 71–82.
  47. Takahashi, K., Igarashi, T., Miyake, K., Kobayashi, M., Yaguchi, C., Iijima, O., Yamazaki, Y., Katakai, Y., Miyake, N., Kameya, S., et al. (2017). Improved Intravitreal AAV-Mediated Inner Retinal Gene Transduction after Surgical Internal Limiting Membrane Peeling in Cynomolgus Monkeys. *Mol. Ther.* 25, 296–302. <https://doi.org/10.1016/j.ymthe.2016.10.008>.